REVIEW ARTICLE

Influence of Operating Parameters on Plasma-Assisted Dry Reforming of Methane in a Rotating Gliding Arc Reactor

Jennifer Martin-del-Campo[1,2] · Sylvain Coulombe[1] · Jan Kopyscinski[2]

Abstract

The environmental impact of greenhouse gases such as carbon dioxide and methane can be reduced if they are used as feedstock to synthesize chemical building blocks such as syngas (CO, H_2) via dry reforming. Methane dry reforming is investigated using an $Ar/CO_2/CH_4$ rotating gliding arc (RGA) reactor powered by a dual-stage pulsed DC power supply. Tangential gas injection combined with a static magnetic field enabled the rotation and upward displacement of the arc along the conical cathode and the grounded anode, yielding to a larger plasma volume. Different parameters such as peak arc current (0.74 and 1.50 A), total gas flow rate (3.7, 4.7 and 6.7 SLPM), CO_2/CH_4 ratio (1.0, 1.5, 2.0) and gas inlet preheating (room temperature, 200 °C) were studied to determine the most efficient parameter combination. Gas conversion was measured online using a calibrated mass spectrometer and offline using a gas chromatograph. Noticeable increases in CO_2 and CH_4 conversions, as well as H_2 and CO yields, were obtained when doubling the peak arc current. For the larger peak current, higher H_2 yields were obtained at a $CO_2/CH_4 = 1.0$, and the best energy efficiencies were obtained at the lowest specific energy input values. No significant effect of the gas inlet temperature on the conversions or yields was found. Trace amounts of acetylene and ethylene, as well as some carbon deposits were observed as by-products of syngas generation. The low amount of by-products obtained implies a good selectivity for CO and H_2, i.e., a cleaner syngas when produced with RGA discharge.

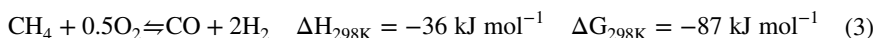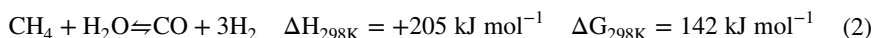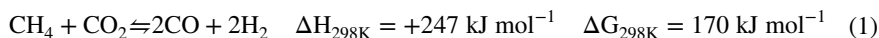**Keywords** Rotating gliding arc · Warm plasma · Dry reforming of methane

✉ Jan Kopyscinski
jan.kopyscinski@mcgill.ca

1   Plasma Processing Laboratory, Department of Chemical Engineering, McGill University, Montreal, QC, Canada

2   Catalytic Process Engineering, Department of Chemical Engineering, McGill University, Montreal, QC, Canada

Introduction

The world is moving towards the use of greener and renewable technologies to meet the ever increasing energy demand; however, fossil fuels are still important in our current energy mix [1]. With the dependence on fossil fuels, the emission of pollutants, such as greenhouse gases (GHG) is an unavoidable problem [2]. Climate change is the major consequence of the enormous amount of greenhouse gases released to the atmosphere, with global and local effects such as an increase in the atmospheric temperature, massive ice melting, ocean acidification, and an enhanced rate of violent localized atmospheric events [3–5]. Carbon dioxide (CO_2) and methane (CH_4) are two of the most significant GHG. Reducing carbon emissions is the most desirable way, but closing the loop on carbon through capture, storage, and utilization is another promising avenue. Dry reforming of methane (DRM) is a reaction that upcycles these two GHG to form syngas, which consists of carbon monoxide (CO) and hydrogen (H_2) (Eq. 1). Syngas can subsequently be converted into liquid hydrocarbons and value-added chemicals for diverse applications. Today, syngas is produced industrially mainly by steam reforming (Eq. 2) and partial oxidation of methane (Eq. 3).

$$CH_4 + CO_2 \leftrightharpoons 2CO + 2H_2 \quad \Delta H_{298K} = +247 \text{ kJ mol}^{-1} \quad \Delta G_{298K} = 170 \text{ kJ mol}^{-1} \quad (1)$$

$$CH_4 + H_2O \leftrightharpoons CO + 3H_2 \quad \Delta H_{298K} = +205 \text{ kJ mol}^{-1} \quad \Delta G_{298K} = 142 \text{ kJ mol}^{-1} \quad (2)$$

$$CH_4 + 0.5O_2 \leftrightharpoons CO + 2H_2 \quad \Delta H_{298K} = -36 \text{ kJ mol}^{-1} \quad \Delta G_{298K} = -87 \text{ kJ mol}^{-1} \quad (3)$$

Even if DRM is thermodynamically the most unfavorable reaction (Eq. 1), it is also the most environmentally friendly due to the use of CO_2 as oxidizing agent [6]. Moreover, sources with large amounts of CO_2 such as biogas can be used from the feed gas without previous separation in the DRM process [7, 8]. Nonetheless, one of the major drawbacks of DRM is that it is a highly energy-intensive process as the C–H bond in methane and C–O bond in carbon dioxide are very stable. Thus, for a thermocatalytic conversion process, high temperatures (> 800 °C) and an efficient catalyst, resistant to coke and carbon deposition, are required [7, 9, 10]. CO_2 and CH_4 can also be activated by means of plasma technology (e.g., non-thermal plasma) that can assist the reaction by providing energy to the highly endothermic process as energetic species such as electrons, ions, free radicals intervene in the chemical reactions and hence, reduce the activation barrier of CO_2 and CH_4 [7, 11]. Additionally, in an increasing number of countries, plasma reactors can be powered by renewable electricity, thus offering a new route for renewable electricity-to-gas processes and applications (e.g., intermittent energy storage and valorization). Plasma technologies such as dielectric barrier discharge (DBD) [12–16], glow discharges [17, 18], microwave discharges (MW) [11], corona discharges [19, 20], radio-frequency discharges (RF) [21] and gliding arc discharges [7, 8, 22–25] have been extensively investigated for reforming reactions. However, corona discharges and dielectric barrier discharges present high energy cost of syngas (> 10 kWh m^{-3}) and low energy efficiency (< 10%) in biogas reforming [26, 27]. On the other hand, RF and MW discharges need to operate at low pressure to achieve high conversions and good hydrogen selectivity but with low hydrogen rate and extra energy cost. Moreover, MW technologies are hard to scale up due to the inherently complicated configurations and high installation costs [28, 29]. A promising technology, the gliding arc discharge, produces a plasma classified by some authors as a

"warm plasma" [26, 30, 31]. Gliding arc discharges present properties between thermal and non-thermal plasmas, such as high electron temperatures (> 1 eV), high electron density of 10^{13}–10^{15} cm^{-3}, and gas temperatures of 1000 to 3000 K, while the non-equilibrium between electrons and heavy particles is still maintained enabling conversion and selectivity [30–33]. Furthermore, up to 45% of the electrical energy provided to the gliding arc may be directly absorbed by endothermic chemical reactions, as in the case of DRM. In fact, without any catalyst, the gliding arc allows the generation of syngas at low temperatures (475 °C) and chemical efficiency (ratio of energy required to carry out the reaction at 25 °C to the used electrical energy) up to 40% [34]. These features make the gliding arc discharge a promising plasma source to satisfy high productivity and good adaptability for plasma-assisted chemical processes [7].

The rotating gliding arc (RGA) is a configuration that makes more efficient use of the energy and arc-cold gas contact, and that is consequently better adapted to scale-up than the traditional knife-shaped gliding arc. In the RGA, the reactant gas is injected tangentially to form a swirling flow field in the reactor. As the arc is pushed away from the breakdown area, it swirls and elongates, thus forming a larger plasma reaction volume compared to the conventional gliding arc. In addition, the arc can be forced to rotate by the action of an external magnetic field through the Lorentz force [33, 35]. The RGA provides a homogeneous distribution of active species in the plasma zone [35, 36].

In this article, a RGA discharge co-driven by tangential gas injection and an external magnetic field was used for dry reforming of methane. Different parameters such as total flow rate, CO_2 to CH_4 stoichiometric ratio, peak arc current, and gas inlet temperature were varied to determine the most efficient parameters combination for DRM. Product gas composition was determined using a calibrated mass spectrometer and gas chromatograph. The influence of the operating parameters on RGA power, specific energy input, and energy efficiency are discussed. Optical emission spectroscopy was used to determine qualitatively the reactive species interacting in the plasma discharge. Scanning emission microscopy and Raman spectroscopy were used to analyze the deposited carbon on the electrodes after the reaction.

Experimental

An adapted version of the rotating gliding arc (RGA) reactor from [37] was developed. The RGA reactor consists of a vertically-mounted conical electrode of 38.5 mm height, which acts as a cathode mounted coaxially inside a hollow cylinder that acts as a grounded anode (Fig. 1). The electrodes are made of stainless steel 316, with a shortest inter-electrode gap of 2.16 mm, increasing to 8.76 mm in the downstream direction. The angle of the cone cathode is 12.2°, and the maximum and minimum diameters are 14.7 mm and 1.5 mm, respectively. The inner diameter of the anode tube is 19.05 mm, with a wall thickness of 9.5 mm, and a total length of 482.6 mm. The reactor is mounted on two pieces that provide electrical insulation between the electrodes. First, a ceramic base (glass-mica) and second, a polyoxymethylene (Delrin™) plate. On the upper part, the reactor is terminated with a ConFlat (CF) tee adaptor that enables direct line-of-sight view along the reactor axis (from the top), and gas exhaust on the side. The plasma-forming gas mixture is injected tangentially through the reactor by two sets of three equally-spaced and angled gas injectors covering the circumference of the reactor (the two sets are separated by 10 mm). The gas injectors are mounted at an angle of 20° axially and 30° radially to the system, providing

**(a)**   **(b)**   **(c)**
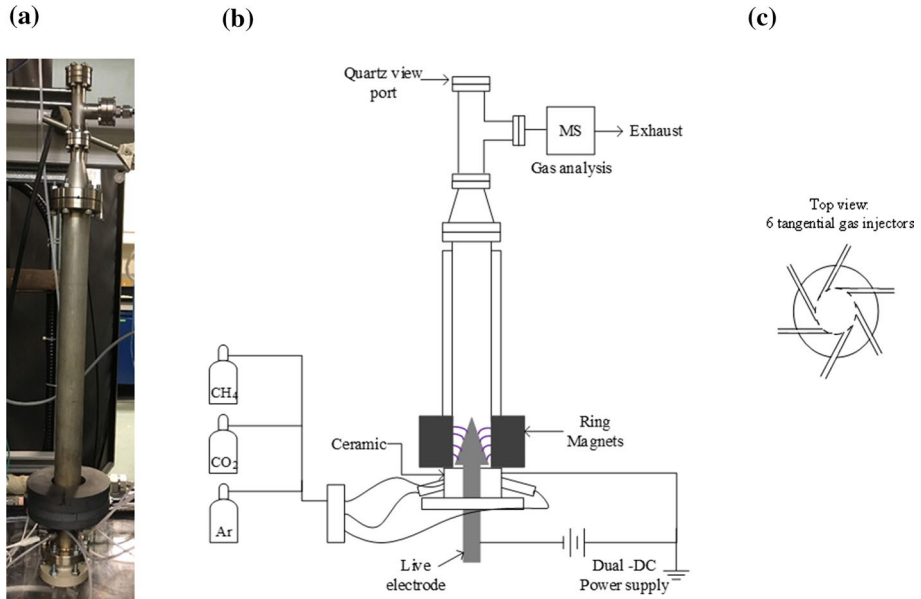
Fig. 1 RGA setup. **a** Photograph of the RGA reactor. **b** Schematics of the RGA setup and **c** six tangential gas injectors configuration (top view)

a counter-clockwise vortex flow up and around the cathode cone (as viewed from the top viewport). No external heating is provided to the reactor. The live cone cathode is powered by a custom-built dual-stage pulsed DC power supply consisting of a high-voltage arc igniter (peak voltage $\sim -$ 4.5 kV) and a current driver power supply (maximum ouput voltage of $-$ 1000 V). The arc igniter consists of a Cockcroft–Walton (CW) voltage multiplier that converts a low-voltage high-frequency AC signal to a pulsed high-voltage negative DC signal. The current driver consists of a resistor–capacitor (RC) circuit driven by a 2.5 kW negative polarity capacitor-charging power supply with a $-$ 1000 V open-circuit voltage [37]. Once the breakdown of the gas is achieved by the arc igniter at the shortest inter-electrode gap, the current driver provides the necessary current to the system and enough voltage for the arc to elongate and be sustained along the live electrode. During the elongation stage, the voltage rises while the current falls, resulting in a typical negative voltage–current characteristic of an arc. A stack of four ring magnets mounted around the anode cylinder adds a static axial magnetic field. The magnets are oriented such as to provide a Lorentz force along the gas drag force [37].

The RGA voltage and circuit current signals were measured online using a high-voltage probe (B&K Precision PR55) and a passive voltage probe (Tektronix P2200) across a 1 Ω shunt resistor, respectively, and displayed/recorded with a digital oscilloscope (PicoScope 2207B). The exhaust gas was analyzed online by a calibrated mass spectrometer (Pfeiffer Ominstar GSD 301), and offline by a gas chromatograph (Agilent 6890N, PLOT-Q Molesieve column) equipped with a thermal conductivity detector (TCD). A mix of gas containing Ar (99.998%, MEGS Specialty Gases), CO_2 (99.9%, MEGS Specialty Gases), and CH_4 (99.99%, MEGS Specialty Gases) was used. To ensure stable plasma operation, the Ar concentration was fixed at 70 vol%. The volumetric CO_2/CH_4 ratios were 1.0, 1.5, and 2.0, with total flow rates of 3.7, 4.7, and 6.7

Fig. 2 Characteristic RGA discharge voltage, current and instantaneous power signals for DRM reaction at $CO_2/CH_4 = 1.0$, 3.7 SLPM, and peak arc current of 1.50 A
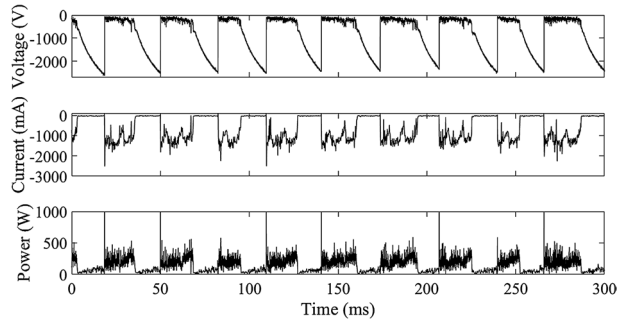
Table 1 Residence times in the RGA discharge zone for different total flow rates

Total flow rate (SLPM)	θ (ms)
3.7	~110
4.7	~86
6.7	~61

SLPM. The maximum current delivered by the current driver was set by changing its internal resistance (1075 Ω, 535 Ω), giving rise to two peak arc current values of 0.74 and 1.50 A, with peak arc power levels of 595 and 1196 W, respectively. Each experiment was conducted 3 times, and the error bars reported were calculated as the standard error of the mean. Typical voltage, current, and calculated instantaneous power (Eq. 13) signals are reported in Fig. 2 for $CO_2/CH_4 = 1.0$, total gas flow rate of 3.7 SLPM, and a peak arc current of 1.50 A. For these conditions, the average pulsing frequency was 28 Hz for a pulse duration of ~16 ms.

The gas residence time in the plasma zone (θ) was estimated as the volume accessible for the plasma (Eq. 4) divided by the volumetric flow rate (Q), and the values are shown in Table 1.

$$V_{plasmazone} = \pi r_1^2 h - \frac{1}{3}\pi h\left(R^2 + r_2^2 + Rr_2\right) \tag{4}$$

where $r_1 = 9.525$ mm is the inner radius of the ground electrode, $R = 7.366$ mm and $r_2 = 0.762$ mm are the larger and small radii of the cone, and $h = 30.48$ mm is the height of the cone electrode.

The calculation of the accessible volume in the plasma zone was made by assuming that the arc goes upwards along all the height of the cone, considering the same value of height for the ground electrode.

Carbon and coke deposition on the electrodes was observed during the reforming reaction. Cyclic reforming-cleaning protocols were developed to avoid the build-up of soot inside the reactor during long experimental runs. The RGA was operated for 15 min under reforming conditions, followed by 5 min Ar/CO_2 cleaning periods (methane flow was turned off while the other flows were kept at the same level, under the same plasma conditions). Lesueur et al. [38] also reported the introduction of CO_2 in a gliding arc reactor to burn off the soot produced in pure CH_4. The cleaning stage enabled the reverse Boudouard reaction (Eq. 5) to take place and proven to be enough to remove the accumulated solid

carbon deposits, as carbon oxidizes to produce CO (observed by mass spectra analysis; not reported here).

$$CO_2 + C_{(s)} \rightleftharpoons 2CO \tag{5}$$

The performance of the reforming reaction was calculated based on hydrogen and carbon monoxide yields (Eqs. 6, 7), and the conversions of methane and carbon dioxide (Eqs. 8, 9):

$$Y_{H_2}(\%) = \frac{\dot{n}_{H_{2_{out}}}}{2 \cdot \dot{n}_{CH_{4_{in}}}} \times 100 \tag{6}$$

$$Y_{CO}(\%) = \frac{\dot{n}_{CO_{out}}}{\dot{n}_{CO_{2_{in}}} + \dot{n}_{CH_{4_{in}}}} \times 100 \tag{7}$$

$$X_{CH_4}(\%) = \frac{\dot{n}_{CH_{4_{in}}} - \dot{n}_{CH_{4_{out}}}}{\dot{n}_{CH_{4_{in}}}} \times 100 \tag{8}$$

$$X_{CO_2}(\%) = \frac{\dot{n}_{CO_{2_{in}}} - \dot{n}_{CO_{2_{out}}}}{\dot{n}_{CO_{2_{in}}}} \times 100 \tag{9}$$

The yield of minor byproducts such as acetylene was calculated as:

$$Y_{C_2H_2}(\%) = \frac{\dot{n}_{C_2H_{2_{out}}}}{\dot{n}_{CO_{2_{in}}} + \dot{n}_{CH_{4_{in}}}} \times 100 \tag{10}$$

The H_2/CO molar ratio and the carbon balances were defined as:

$$\frac{H_2}{CO} = \frac{\dot{n}_{H_{2_{out}}}}{\dot{n}_{CO_{out}}} \tag{11}$$

$$B_C(\%) = \frac{\dot{n}_{CO_{2_{out}}} + \dot{n}_{CH_{4_{out}}} + \dot{n}_{CO_{out}}}{\dot{n}_{CO_{2_{in}}} + \dot{n}_{CH_{4_{in}}}} \times 100 \tag{12}$$

where $\dot{n}_i$ is the molar flow rate in (mol min^{-1}). The quantity of other hydrocarbons (C_2H_2, C_2H_4) was rather small (<0.5 mol%) and was neglected in the carbon balance.

The instantaneous power $P(t)$ was calculated by multiplying the voltage $V(t)$ and current $I(t)$ (Eq. 13):

$$P(t) = V(t)I(t) \quad [W] \tag{13}$$

The evolution of the cumulative energy deposited in the RGA up to time t, $E(t)$, was calculated by integrating the product of the arc voltage $V(t)$ and circuit current $I(t)$ signals (Eq. 14):

$$E(t) = \int_0^t V(t)I(t)dt \quad [\text{J}] \tag{14}$$

By determining the slope of the cumulative energy curve (assuming a linear trend, validated with Fig. 12), the time-average power was determined, which can also be obtained by Eq. (15):

$$P_{avg} = \frac{1}{T} \int_0^T P(t)dt \quad [\text{W}] \tag{15}$$

where T is the total time frame observed (typically 1 s).

The specific energy input (SEI) defines the amount of energy input per mol of gas injected, defined as:

$$SEI = \frac{P_{avg}}{\dot{n}_{reactants}} \quad \left[\text{kJ mol}^{-1}\right] \tag{16}$$

where $\dot{n}_{reactants}$ is the molar flow rate of CO_2 and CH_4.

The energy efficiency (η) of the process was defined as the ratio of the chemical energy from the products (H_2 and CO) to the energy given to the system, i.e., CH_4 and power input (Eq. 17)

$$\eta(\%) = \frac{\dot{n}_{H_{2_{out}}} LHV_{H_2} + \dot{n}_{CO_{out}} LHV_{CO}}{P_{avg} + \dot{n}_{CH_{4_{in}}} LHV_{CH_4}} \times 100 \tag{17}$$

where LHV_i stands for the Low Heating Value of the species in (J mol^{-1}).

Optical emission spectroscopy (OES) was used to identify reactive species in the plasma for the DRM reaction. Optical emission spectra were logged using an Ocean FX spectrometer (Ocean Optics, 25 μm slit, extended range 200–1100 nm) with an optical resolution of 0.78 nm. The integration time per scan was 300 ms, and the resulting spectrum was the average of 5 scans. Scanning emission microscopy (SEM) (Hitachi SU8000) was performed on samples of the deposited solid carbon with an accelerating voltage of 10 to 20 kV, and working distance between 5.4 and 15.4 mm. In addition, Raman spectroscopy (Bruker SENTERRA confocal) with a wavelength of 532 nm was used to analyze the solid carbon samples collected after approximately 20 h of processing.

Results and Discussion

Thermodynamic Analysis

Dry reforming of methane involves the most oxidized form of carbon, CO_2, combined with its most reduced form, CH_4, (Eq. 1). In DRM, carbon dioxide can be considered as a soft oxidizing agent [39]. As an oxidant, it requires significant energy to activate the molecule in order to interact. Since CO_2 is a stable molecule, DRM is a highly endothermic reaction [6]. Figure 3 shows the equilibrium composition as a function of

Fig. 3 Equilibrium composition of DRM as a function of temperature for $CO_2/CH_4 = 1.0$, 1.5, and 2.0 at 1 bar. Note the absolute composition of Ar (in mol) is constant throughout the whole temperature range. Hence, Ar is not reported in the graphs
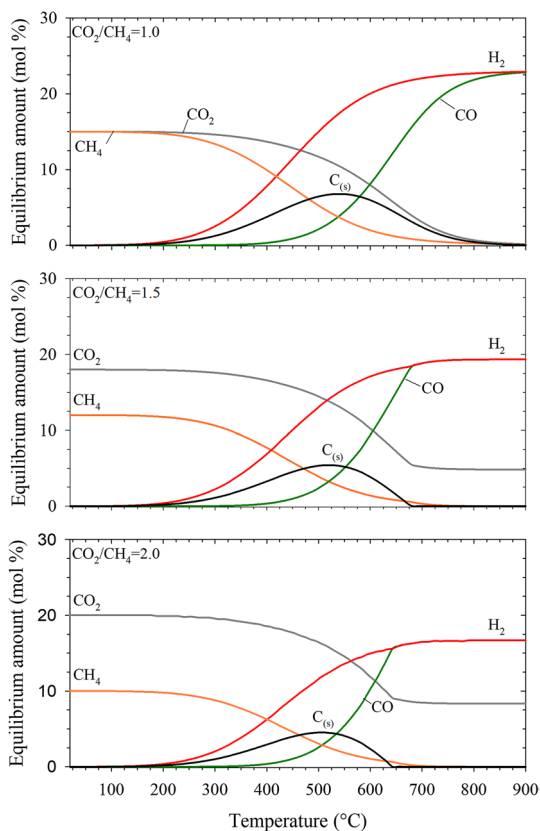
temperature for the DRM based on the minimization of Gibbs energy (HSC Chemistry 9) for $CO_2/CH_4 = 1.0$, 1.5, and 2.0 at 1 bar. The main products included in the reaction are CH_4, CO_2, H_2, CO, and $C_{(s)}$. Water was not included in the thermodynamic calculations as it was not observed during the reaction (no peak of OH in OES spectra). The concentration of other byproducts such as C_2H_2 and C_2H_4 are negligible (> 0.01%) and are not reported. Noticeable CH_4 conversion is obtained at 375 °C (22 to 26%) for all the stoichiometric ratios. On the other hand, the conversion of CO_2 is favored at temperatures > 500 °C. Increasing CO_2/CH_4 ratio leads to an increase in CH_4 conversion, especially meaningful above 400 °C. For instance, the conversion of CH_4 increases 1.17 times when the CO_2/CH_4 ratio increases from 1.0 to 2.0 at approx. 420 °C. Conversely, CO_2 acts as the limiting reactant for the conversion of CH_4 at $CO_2/CH_4 = 1.0$, leaving 1% of CH_4 unreacted at 900 °C.

Hydrogen production is limited by the amount of CH_4 injected in the feed, as less CH_4 is available for dehydrogenation. Whereas the production of H_2 starts to be appreciable at 250 °C (4 to 5%), CO yield starts to be noticeable above 450 °C (3 to 4%) for all CO_2/CH_4 ratios. Conversely, the H_2/CO ratio decreases with increasing temperature for all CO_2/CH_4 ratios. In addition, at $CO_2/CH_4 = 2.0$, an equimolar H_2-CO mix is obtained at lower temperatures (650 °C) compared to temperatures > 900 °C for $CO_2/CH_4 = 1.0$.

On the other hand, a higher concentration of CO_2 in the mixture leads to a decrease in solid carbon formation. For instance, higher solid carbon formation can be found at

$CO_2/CH_4 = 1.0$ at 550 °C (6.7%), compared to $CO_2/CH_4 = 1.5$ (5.1%) and $CO_2/CH_4 = 2.0$ (4.0%) at the same temperature. Moreover, the temperature for maximum carbon formation is shifted from 550 to 500 °C when the CO_2/CH_4 increases from 1.0 to 2.0. Higher concentrations of CH_4 in the feed favor the methane cracking reaction ($CH_4 \leftrightarrow C_{(s)} + 2 H_2$) and lead to (a) higher carbon deposition, and (b) higher temperature where the solid carbon can be suppressed. By increasing the CO_2/CH_4 from 1.0 to 2.0, solid carbon formation can be suppressed > 650 °C instead of at > 875 °C.
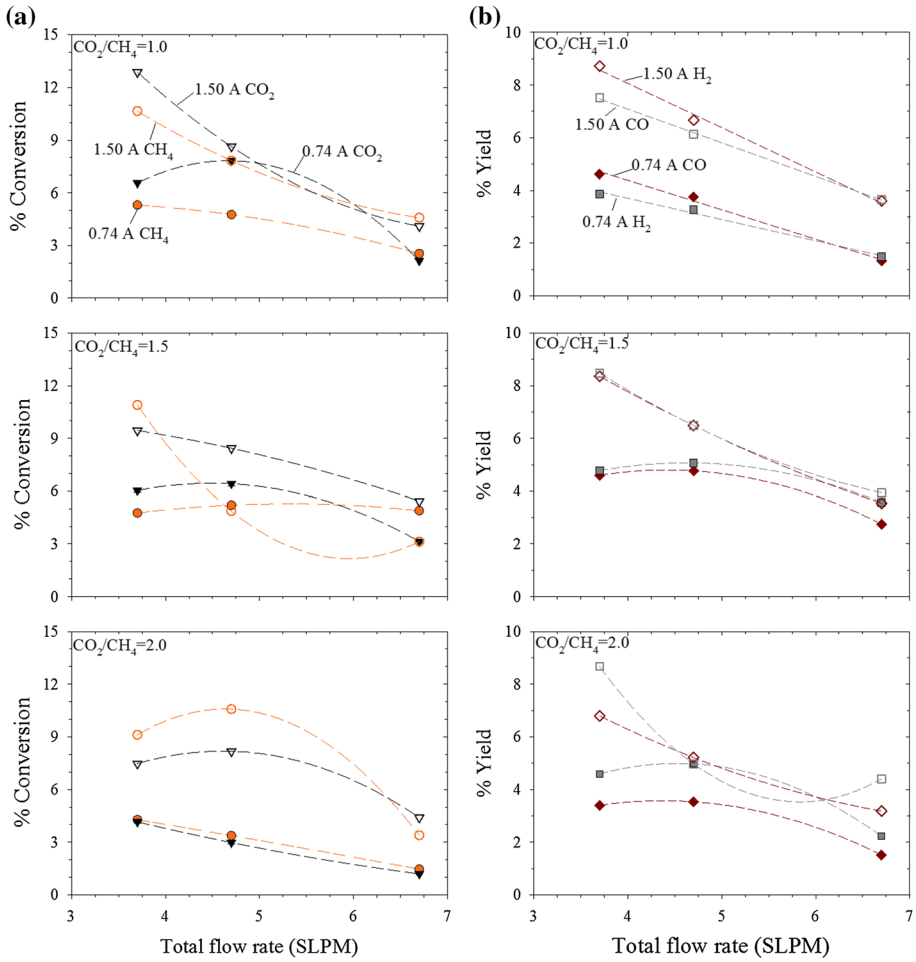
Conversion and Yield

Hydrogen and carbon monoxide were the main products obtained by DRM, while solid carbon (C), as well as C_2-species such as acetylene (C_2H_2) and ethylene (C_2H_4), were minor by-products ($< 1\%$ yield). The latter were observed in considerably smaller amounts when compared to other plasma sources, such as DBDs [7, 24, 40], which can be explained by a higher electron density in the rotating gliding arc lowering the activation energy and yielding a clean syngas.

The temporal evolution of the conversion of CO_2 and CH_4, as well as the yield of CO, was similar to the presented hydrogen yields (Fig. 5) and is not reported in this article. The average conversions of CO_2 and CH_4, as well as the H_2 and CO yields at steady-state are reported in Fig. 4a, b, respectively. At lower stoichiometric ratios of CO_2/CH_4, the amount of CO_2 converted was higher than the CH_4 for total gas flow rates of 3.7 and 4.7 SLPM. Conversely, when the total flow rate was increased to 6.7 SLPM, CO_2 and CH_4 conversions had mostly the same values, independently of the peak current or the stoichiometric ratio. When the peak current was set at 0.74 A, the CO_2 conversion reached a maximum value when the total flow rate increased from 3.7 to 4.7 SLPM and decreased afterwards for $CO_2/CH_4 = 1.0$ and 1.5. According to Zhang et al. [32], under certain conditions, the increase of flow rate could improve the CO_2 conversion in a RGA, which probably directs to the CO_2 activation into a more efficient pathway through vibrational excitation. Besides, increasing the total flow rate leads to an increase in the length of the arc, which enhances the conversion rate [41].

On the other hand, doubling the peak current from 0.74 to 1.50 A also increased the plasma input power, and consequently the electron density and gas temperature. These parameters can influence CO_2 and CH_4 conversions in different ways [7]. When the peak current doubled from 0.74 to 1.50 A for a total flow rate of 3.7 SLPM, an increase in CO_2 and CH_4 conversion was particularly evident at $CO_2/CH_4 = 2.0$. Under these conditions, the extent of CO_2 and CH_4 conversion increased 1.8 and 2.1 times, respectively. Similarly, at 4.7 SLPM, the CO_2 and CH_4 conversion increased from 3.0 and 3.4% to 8.2 and 10.6%, respectively, which represented increments of 2.7 and 3.1 times. By further increasing the flow rate to 6.7 SLPM, the conversion of CO_2 increased 3.7 times when the current increased from 0.74 to 1.50 A. A similar trend for the conversion of CO_2 and CH_4 can be observed for $CO_2/CH_4 = 1.0$; however, in the case of CO_2 only an increment of 10% for 4.7 SLPM was obtained when the current doubled from 0.74 to 1.50 A. The co-feeding of CH_4 and CO_2 has a synergistic effect in the conversion of each other [42]. As mentioned before, CO_2 is a soft oxidant that first dissociates into CO and O radicals (Eq. 18), generating some oxygen species, such as metastable O (^{1}D). Reactive oxygen species can break the C-H bond and generate methyl and hydroxyl radicals from CH_4 [7, 42].

Hydrogen yields as a function of time for two different peak current levels at $CO_2/CH_4 = 1.0$ are depicted in Fig. 5. These yields vary with time, presenting a transient behavior in the first

Fig. 4 **a** Average conversions of CO_2 and CH_4 and **b** average yields of H_2 and CO as a function of total gas flow rate for peak arc currents of 0.74 and 1.50 A. Dashed lines are used only for guidance. Note that the error bars are smaller than the symbols
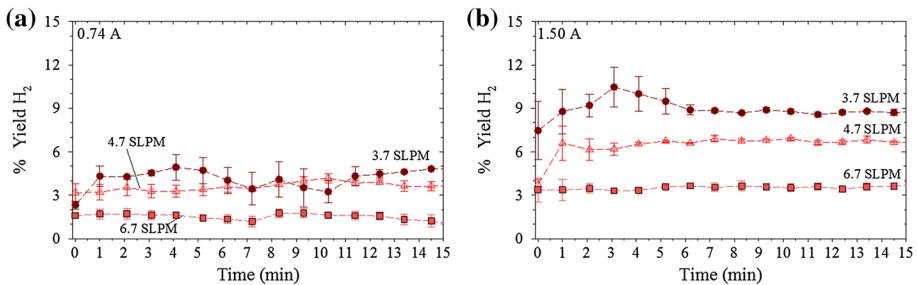
Fig. 5 Temporal evolution of H2 yields at peak currents of **a** 0.74 and **b** 1.50 A, for $CO_2/CH_4 = 1.0$ and total flow rates of 3.7, 4.7, 6.7 SLPM. Dashed lines are used only for guidance

minutes, i.e., reaching a maximum value (and more variability) between 3 and 5 min and stabilizing afterwards, with constant values and low variability. This finding could be helpful in determining the more convenient time to measure gas concentrations with consistent results, especially with offline measurements. On the other hand, an increase in yield was observed when the peak arc current was doubled. A higher arc current is associated with a higher electron density, thus providing high rates for breaking the strong C-O and C-H bonds, resulting in higher conversions of CO_2 and CH_4 and higher production of CO and H_2.
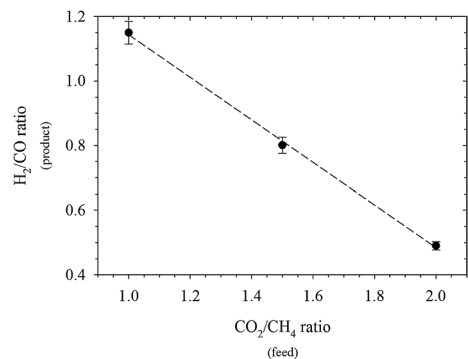
The residence time in the RGA discharge zone is a function of the total flow rate, whereas a higher total gas flow rate means a lower gas residence time in the plasma zone (Table 1), hence less time for CO_2 and CH_4 to react and collide with electrons and active species to produce syngas. This effect was clearly seen with the peak arc current of 1.50 A, where higher H_2 and CO yields at lower total flow rates were obtained. However, when the peak arc current was 0.74 A, there was almost no observable effect of the total flow rates of 3.7 and 4.7 SLPM on the yields. In addition, increasing the total flow rate from 3.7 to 6.7 SLPM decreased CO_2 and CH_4 conversions. When the CO_2/CH_4 ratio was set to 1.0, a high concentration of H_2 was observed, as more CH_4 was available for dehydrogenation. Equally, when the CO_2/CH_4 ratio was set to 2.0, there was a higher production of CO. Once steady state was achieved, the maximum values of H_2 and CO obtained with a peak arc current of 1.50 A and 3.7 SLPM were 8.7% for both H_2 and CO at CO_2/CH_4 of 1.0 and 2.0, respectively.
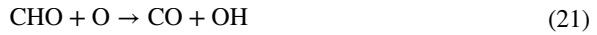
The total gas flow rate and peak arc current had a stronger influence on DRM than changing the CO_2/CH_4 ratio. The CO_2/CH_4 ratio did not affect the DRM reaction significantly, but influenced the H_2/CO ratio, as shown in Fig. 6. Controlling the H_2/CO ratio in syngas might be useful for valorization purposes [43], as it influences the downstream process. For instance, syngas very rich in CO is valuable for the production of oxygenated chemicals [12, 44]. In Fig. 6, the error bars represent the standard error of the mean considering the variations between the different flow rates and peak currents. The CO_2/CH_4 ratio presented an inversely proportional behavior to the H_2/CO_2 ratio, i.e., the higher the CO_2 concentration in the feed mixture, the lower the amount of H_2 produced, as less CH_4 was available for dehydrogenation. There was no significant effect of the peak arc current or the total flow rate on the H_2/CO ratio.

Carbon monoxide is mainly formed via dissociation of CO_2 (Eq. 18) upon collision with electrons [45, 46]. Recombination of radicals in the reactive plasma can lead to the formation of carbon monoxide (Eqs. 19–21) and carbon dioxide (Eq. 22). Some of the elementary steps for CO and CO_2 formation are stated by the following equations [12, 23]:
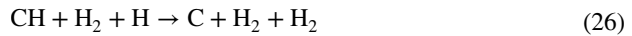
$$CO_2 \rightarrow CO + O \tag{18}$$

Fig. 6 Influence of the CO_2/CH_4 ratio on the H_2/CO ratio, the symbols represent the average values. Dashed lines are used only for guidance

$$CHO + H \rightarrow CO + H_2 \tag{19}$$

$$CHO + OH \rightarrow CO + H_2O \tag{20}$$

$$CHO + O \rightarrow CO + OH \tag{21}$$

$$CHO + O \rightarrow CO_2 + H \tag{22}$$
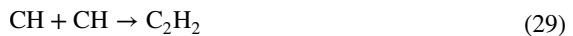
The dissociation of methane by electron collisions produces the CH_3 radical that by further dissociation produces hydrogen. Some of the reactions leading to H_2 production are stated by Eqs. (23–28) [12, 23]

$$CH_4 + H \rightarrow CH_3 + H_2 \tag{23}$$

$$CH_2 + H + H \rightarrow CH_2 + H_2 \tag{24}$$

$$CH_2 + H_2 \rightarrow CH + H_2 + H \tag{25}$$

$$CH + H_2 + H \rightarrow C + H_2 + H_2 \tag{26}$$

$$OH + H \rightarrow O + H_2 \tag{27}$$

$$OH + H \rightarrow O + H_2 \tag{28}$$

Trace amounts of acetylene were measured in the gas product, which might have been formed via various C–C coupling reactions such as dimerization of radical CH (Eq. 29) or CH_2 with subsequent H_2 elimination (Eq. 30) or via ethylene dehydrogenation (Eq. 33). Ethylene was most likely formed via CH_3 or CH_2 coupling, instead of dehydrogenation of ethane as the latter was not observed with mass spectrometry (Eqs. 34, 35).

Some of the possible reactions for the formation of acetylene are stated by Eqs. (29–33) [23]:

$$CH + CH \rightarrow C_2H_2 \tag{29}$$

$$CH_2 + CH_2 \rightarrow C_2H_2 + H_2 \tag{30}$$

$$CH_2 + CH \rightarrow C_2H_2 + H \tag{31}$$

$$C_2H_3 + H \rightarrow C_2H_2 + H_2 \tag{32}$$

$$C_2H_4 \rightarrow C_2H_2 + H_2 \tag{33}$$

Conversely, possible reactions for ethylene formation are stated by Eqs. (34, 35) [23]:

$$CH_3 + CH_3 \rightarrow C_2H_4 + H_2 \tag{34}$$

Fig. 7 Yield of acetylene concentration for DRM for CO_2/CH_4 ratios of 1.0, 1.5 and 2.0, total gas flow rates of 3.7, 4.7 and 6.7 SLPM, and peak current of 1.50 A.

$$CH_2 + CH_2 \rightarrow C_2H_2 \tag{35}$$
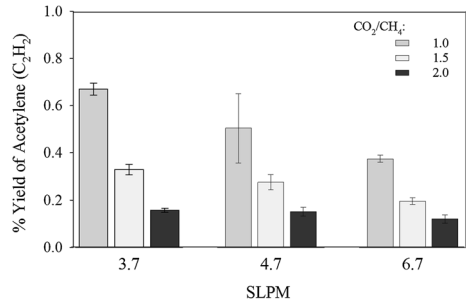
Acetylene production decreased significantly with increasing the CO_2/CH_4 ratio as well as with increasing the total gas flow rate (Fig. 7). For CO_2/$CH_4 = 1.0$, an acetylene concentration of 0.23 mol% was measured, which decreased to less than half (0.11 mol%) at a ratio of 1.5 and decreased further to 0.05 mol% at a ratio of 2.0. The formation of C_2H_2 was directly proportional to the inlet partial pressure of CH_4 with an apparent reaction order of 3.7 ± 0.2 at a flow rate of 3.7 SLPM. At higher flow rates the reaction order in CH_4 decreased to 2.9 ± 0.1 and 2.7 ± 0.3 at 4.7 SLPM and 6.7 SLPM, respectively (see supplementary material A). This implies that increasing the CH_4 partial pressure by a factor of 2 increases the acetylene formation by at least a factor of 8. At a higher total gas flow rate and thus, for lower residence time, less CH radicals and therefore less C_2H_2 were produced. This effect was more pronounced at lower CO_2/CH_4 ratios (i.e., higher CH_4 partial pressure). A small amount (<0.02 mol%) of ethylene (C_2H_4) was measured; however, no clear trend was visible. Especially at high flow rates and low peak currents, no ethylene was observed.

The carbon balance for all the experiments was >95%. Ethylene and acetylene were not considered in the carbon balance due to their small concentrations (<0.25 mol %, <1% yield). The main carbon product was CO, and the C_2 products were more than 100 times less than the CO produced. The low concentrations of byproducts imply good selectivity for H_2 and CO when the DRM is carried out in the rotating gliding arc discharge.
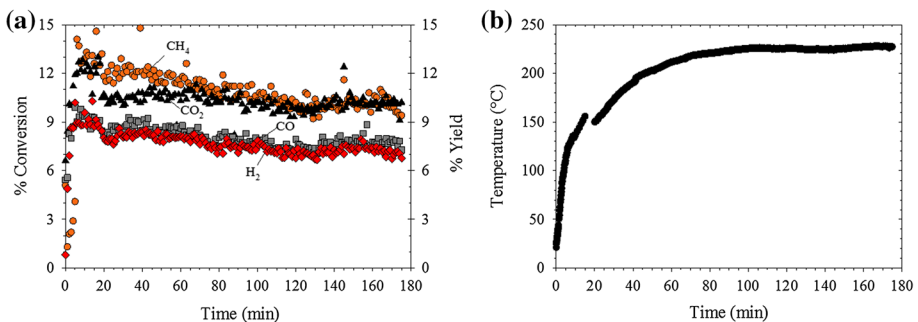
Fig. 8 **a** Conversion of CO_2 and CH_4, and yield of H_2 and CO and **b** temperature profile as a function of time of the DRM at a total flow rate of 3.7 SLPM, CO_2/$CH_4 = 1.5$ and peak current of 1.50 A

A 3 h experiment was carried out in the RGA reactor to determine the temporal evolution of the CO_2 and CH_4 conversions, and the CO and H_2 yields with a total gas flow rate of 3.7 SLPM, CO_2/CH_4 ratio of 1.5 and peak arc current of 1.50 A (Fig. 8a). Initial conversions of 13 and 14% were achieved in the first 10 min for CO_2 and CH_4, respectively. Thereafter, the CO_2 conversion dropped to 10% and stabilized until the end of the 3 h run, while the CH_4 conversion steadily decreased from 14 to 10%. As for CO and H_2, an equimolar amount was observed during the 3 h as per the dry reforming reaction $(CO_2 + CH_4 \rightarrow 2CO + 2H_2)$. This also indicates the absence of water gas shift and steam reforming reactions. The CO and H_2 yields decreased slightly towards the end of the run, most likely due to carbon deposition on the electrodes.

Figure 8b shows the temperature inside the reactor (~76 mm above the cathode, to avoid interactions between the thermocouple and the arcs) as a function of time. The reactor itself was insulated to reduce heat losses through the walls. It took more than 60 min to reach a stable temperature at around 227 °C. The sudden temperature drop of 5 °C between minutes 15 and 20 could be attributed to the energy given to the RGA was mostly transformed into chemical energy, as more CH_4 and CO_2 converted before min. 20, rather than into thermal energy. This thermal induction period in the RGA reactor has been reported by others using non-thermal plasma discharges as well [16, 47–50]. When the RGA discharge was operating, faster heating in the gas was observed because the power was directly applied through the RGA and not through the walls, like in the case of a conventional gas heater. Nonetheless, regardless of the gas heating, the RGA discharge is mostly considered non-thermal or "warm" plasma as the electron temperature is conventionally > 1 eV, whereas the gas temperature could reach 1000–3000 K, but still sustaining a non-equilibrium between heavy particles and electrons [31]. During the first 15 min of operation, there was a rapid increase in temperature, $\Delta T = 135$ °C, while the conversion and yields presented higher values. After 100 min, the reaction temperature achieved steady-state, with a temperature of 227 °C and an overall $\Delta T = 206$ °C. Carbon dioxide and methane are polyatomic molecules with vibrational, translational, and rotational modes. Hence, the kinetic energy transferred from the electrons to the molecules and between the molecules themselves is mainly converted into thermal energy, translating in an increase of temperature. Note that even in the context of a highly endothermic reaction, the increase of the gas temperature did not enhance the performance of the DRM reaction. Actually, CO_2 and CH_4 conversions decreased by 20 and 25%, respectively, when calculated at the beginning of the reaction (between 10 to 15 min) compared to the conversion determined at the end of the reaction (between 170 to 175 min), possibly due to accumulation of carbon deposited on the electrodes. Decreased CO_2 and CH_4 conversions have also been reported by [49] when increasing the temperature in a DBD catalytic reactor, without an explanation provided by the authors.

Effect of Inlet Gas Temperature

Some studies have reported preheating the reactants [30, 40] for DRM in gliding arc discharge, whereas others have carried out the reaction with gases being fed at room temperature [7, 25, 41]. However, the effect of inlet gas temperature on CO_2 and CH_4 conversions and H_2 and CO yields for RGA discharge is still not clear. Maqueo et al. [2] reported that preheating the inlet gas did not affect the plasma-assisted dry reforming reaction in a nanosecond pulsed discharge. Zhou et al. [12] reported that increasing the temperature up to 250°C in a DBD reactor hardly influenced the conversion of
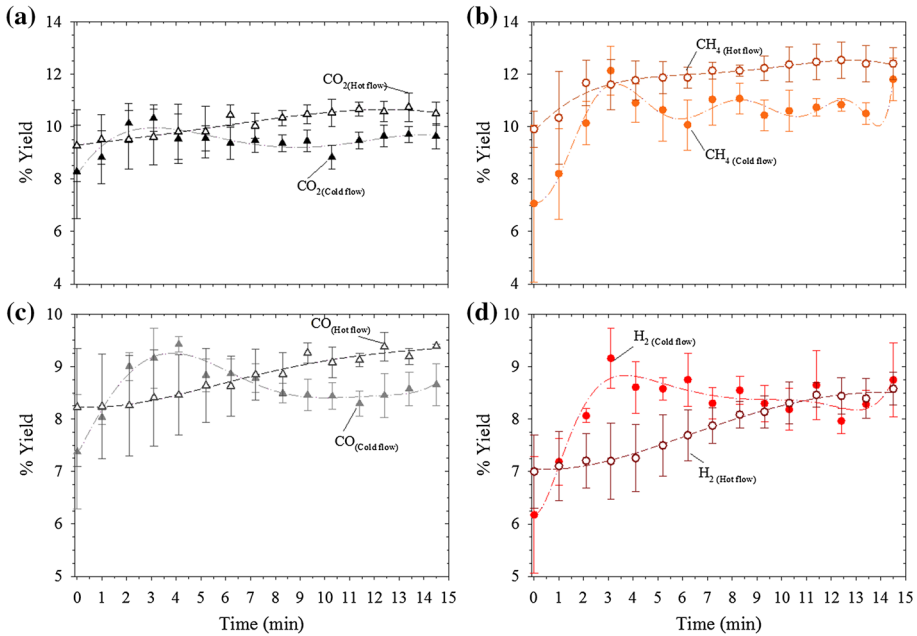
Fig. 9 **a** CO_2 conversion, **b** CH_4 conversion, **c** CO yield and **d** H_2 yield as a function of time for not pre-heated (open symbols) and preheated (full symbols) gas at a total flow rate of 3.7 SLPM, $CO_2/CH_4 = 1.5$, and peak current of 1.50 A. The error bars represent the standard error of the mean. Dashed lines are used only for guidance

CO_2 and CH_4. An ANOVA statistical analysis was performed to the results to determine whether the means of the two groups, i.e., preheated and not-preheated flow, were statistically different from each other (see supplementary material B). Figure 9 shows the conversions of CO_2 and CH_4 and the yields of CO and H_2 as a function of time for non-preheated and preheated (200 °C) inlet gas feeding. The results of the ANOVA tests indicated that there was not enough evidence to state a significant statistical difference between the means of the conversions and yields for pre-heated and not preheated gas inlet. On the other hand, the H_2/CO ratio decreased from 0.86 to 0.77 when the inlet temperature was increased to 200 °C. However, this can still be considered as part of the error reported previously in Fig. 6 (lower limit of error bar).

The energy needed to preheat the inlet flow was provided by a gas heater wrapped with heating tape. Considering the power supplied by the heating tape, the total input power was determined (discussed further in the next section). The input power, i.e., RGA power and power provided by the heating tape, increased from 166 to 590 W (3.5 times more) when the temperature was 200 ºC. Thus, the energy efficiency (Eq. 17) dropped from 8.1 to 4.7%, which represents a drop of 60%, reducing the effectiveness of the process when the temperature was increased from room temperature to 200 °C. As discussed in the previous section, plasma discharges induce gas heating. This result is shown in Fig. 10, where T_1 is the inlet temperature measured in the manifold, before the distribution of the gas through the gas injectors. T_0 was measured during the first 20 min just above the cathode cone (no arcing) and 76 mm above it when the RGA was active. Note that the thermocouple was placed first on top of the cathode cone to the gas

Fig. 10 Gas temperature of the inlet (T_1) and inside the reactor (T_0) versus time for 3 DRM periods separated by two periods of electrode regeneration. Total flow rate of 3.7 SLPM during DRM and 3.26 SLPM during electrode regeneration, $CO_2/CH_4=1.5$, peak current of 1.50 A
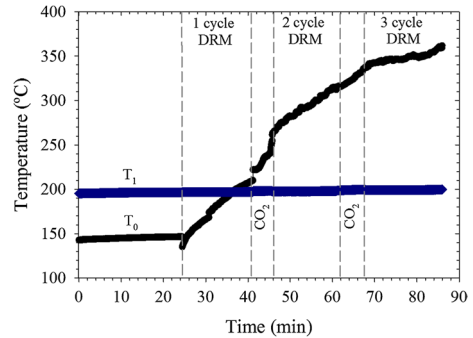
inlet in the reactor to determine the temperature of the gas compared to the temperature measured at the manifold. Then the thermocouple was moved away during the RGA experiment to avoid interactions between the thermocouple and the arcs. Three periods of DRM reaction were carried out at a total flow rate of 3.7 SLPM, $CO_2/CH_4 = 1.5$, and peak arc current of 1.50 A, separated by two periods of electrode regeneration (CH_4 flow was stopped during regeneration phase; hence, total flow rate decreased to 3.26 SLPM).

The gas heating caused by the RGA is clearly seen in Fig. 10. We also noticed that the gas heating appeared to be faster during the regeneration phase (carried out in Ar/CO_2) as the specific heat value of CO_2 ($c_p=0.844$ J g^{-1} K^{-1}) is ~2.6 times lower than for CH_4 ($c_p=2.22$ J g^{-1} K^{-1}). Therefore, more energy was needed to change the temperature of the mix, CH_4 and CO_2, than when the RGA was operating only with CO_2, making the gas heating faster in the last case. Besides, during the regeneration phase there was a decrease of the total flow rate from 3.70 to 3.26 SLPM whilst the RGA was operating at the same power conditions, which also made the gas heating faster during this phase. The overall temperature change associated with RGA heating was $\Delta T_0 = 241$ °C.
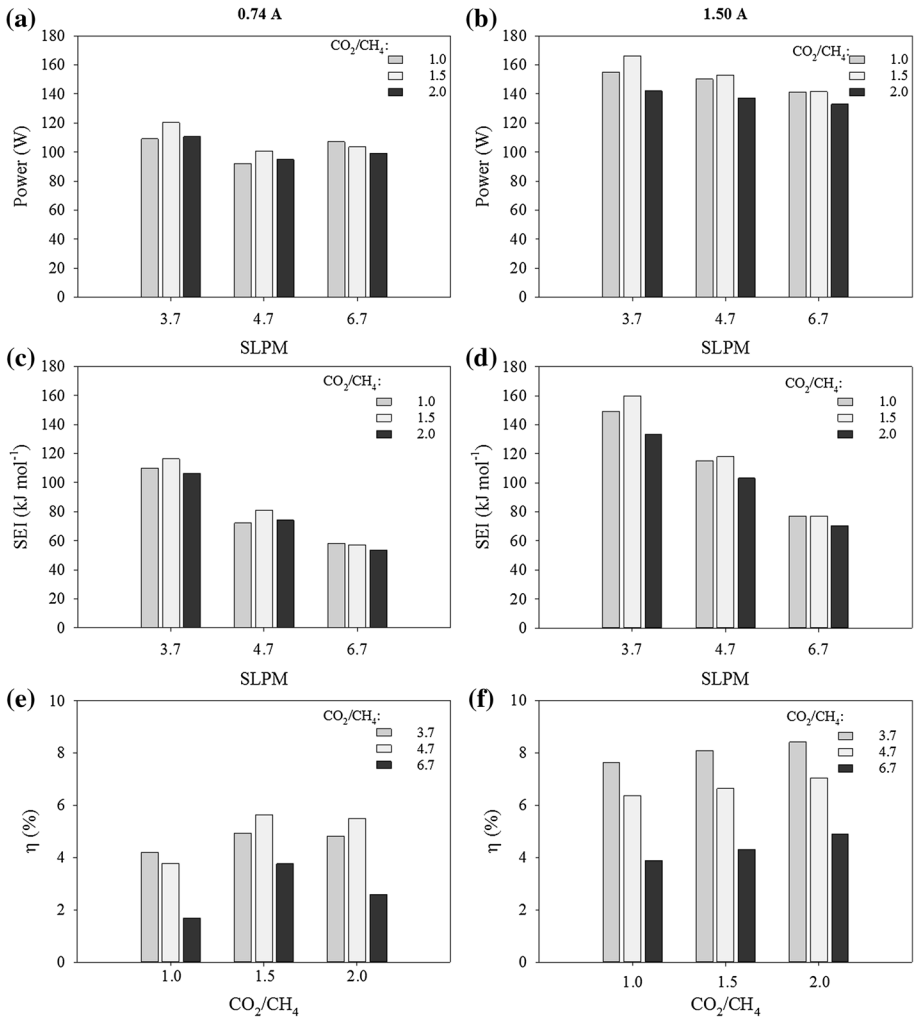
Energy

Figure 11 shows the cumulative energy deposition in the RGA (Eq. 14) over 25 s for DRM with CO_2/CH_4 ratios of 1.0, 1.5 and 2.0 with a total flow rate of 3.7 SLPM and peak arc current of 1.50 A. The trend is linear, revealing the steadiness of the RGA power over this time scale. Using the slope of the cumulative energy lines, average powers (Eq. 15) of 155.0 ± 0.4 W, 166.0 ± 0.5 W, and 142.1 ± 0.6 W were obtained, respectively. This reveals

Fig. 11 Temporal evolution of the accumulated energy deposited for DRM for CO_2/CH_4 ratios of 1.0, 1.5 and 2.0 at a total flow rate of 3.7 SLPM and peak current of 1.50 A
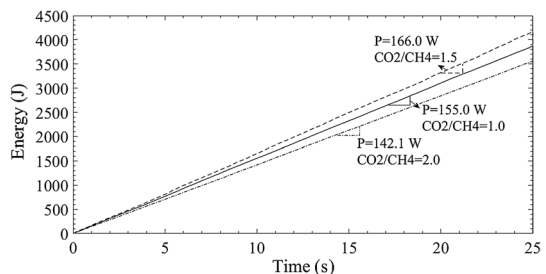
Fig. 12 Power provided to the RGA (**a**, **b**), specific energy input (SEI) (**c**, **d**) and energy efficiency (η) (**e**, **f**) for DRM with CO_2/CH_4 ratios of 1.0, 1.5 and 2.0, total gas flow rate of 3.7, 4.7 and 6.7 SLPM, and peak currents of 0.74 and 1.50 A

that the average power not only changed with the gas composition but also with the total gas flow rate (Figs. 11, 12a, b). The changes between the average powers of the mixtures can be attributed to the differences between the resistivity of the gas mixture and the radiative losses.

An increased RGA current led to an increased deposition of solid carbon on the electrodes and increased the production of C_2H_2. These undesired by-products were not considered in the energy efficiency calculations, which can lead to an underestimation of the overall process efficiency [2]. For instance, considering the carbon balance, approximately 5% of the solid carbon contributes up to ~19.7 kJ for the energy balance. However, only major gas components were considered in the calculation of energy efficiency (Eq. 17). Energy efficiency increased in a range of 1.1 to 2.3 times when the peak arc current was

doubled (Fig. 12e, f), but decreased when the total gas flow rate was increased. This effect can be explained due to the smaller yields of H_2 and CO production as shown in Fig. 4b. The energy efficiency also increased by increasing the amount of CO_2 in the feed, i.e., at higher CO_2/CH_4 ratios, when the current doubled from 0.74 to 1.50 A. At higher RGA current and CO_2/CH_4 ratio in the inlet gas composition, the amount of carbon deposited on the electrodes was lower than in the other cases, which affected not only the reaction products but also the overall energy efficiency. In Fig. 12c, d, the SEI decreased linearly when increasing the total gas flow rate for both peak arc currents and for all stoichiometric ratios. Furthermore, when the arc current was doubled, the best energy efficiencies were obtained at lower SEI values. This effect has also been reported in [51]. In our study, it could be observed that the best energy efficiencies were obtained at $CO_2/CH_4 = 2.0$, and peak current of 1.50 A for each flow rate. These results indicate that higher concentrations of CO_2 in the inlet stream are beneficial for the DRM reaction, most likely as the C–C coupling is hindered due to lower CH_4 partial pressure; consequently, producing less coke. In contrast, when the arc current was set at 0.74 A, the highest energy efficiencies and SEI values were obtained at $CO_2/CH_4 = 1.5$ for all total gas flow rates.

Table 2 shows the percentage of electrical power that contributed to H_2 and CO production. This value was calculated by considering only the power in the denominator of Eq. 17. It can be noticed that the electrical power input contributed in a range of ~ 15 to 30% to the conversion of CH_4 and CO_2 to H_2 and CO. When the current was 0.74 A, there was a higher use of the electrical power input for a total flow rate of 4.7 SLPM, as increasing the flow rate could direct to an increase in the arc length and CO_2 activation into a more efficient pathway, as mentioned before [32, 41], also leading to higher CO production. In the case of the peak current of 1.50 A, there is no significant difference in the percentage of electrical power contribution between the different conditions studied.

Table 3 shows a comparison of the performance parameters for different plasma sources for DRM. It can be noticed that the SEI of the DRM reaction using gliding arc discharges is 4 to 167 times lower compared to other plasma sources such as corona discharges or dielectric barrier discharges. This means that more energy needs to be supplied to the discharge to treat the same amount of gas than for gliding arcs. As a transitional plasma discharge (or warm plasma), gliding arc discharges possess characteristics of thermal and non-thermal plasmas, providing higher gas temperatures and electron densities compared to non-thermal plasmas, but still working under at low current and power density [24, 30, 46]. As reported by [7] the electron density in the gliding arc discharges (10^{23} m^{-3}) is higher compared to corona (10^{15}–10^{19} m^{-3}), glow discharges and DBDs (10^{16}–10^{19} m^{-3}). Hence, it is easier to achieve higher conversions at higher flow rates with GA [24]. The RGA is a promising technology to conduct highly endothermic reactions like the DRM. Improvements in the performance of this plasma source can be achieved by optimizing the power delivery.

Table 2 Percentage of electrical power input that contributed to the H_2 and CO production, for peak currents of 0.74 and 1.50 A, $CO_2/CH_4 = 1.0$, 1.5, 2.0 and total flow rates of 3.7, 4.7 and 6.7 SLPM

CO_2/CH_4	1.0		1.5		2.0	
Total flow rate (SLPM)	0.74 A	1.50 A	0.74 A	1.50 A	0.74 A	1.50 A
3.7	19.8	29.0	19.9	26.1	17.0	26.7
4.7	26.5	30.1	29.8	26.6	26.6	27.1
6.7	14.6	25.7	28.1	24.6	17.0	25.1

Table 3 Comparison of performance parameters for different plasma sources for DRM

Plasma source	Feed flow (mL min^{-1})	CO$_2$/CH$_4$	Conversion (%)		Yield (%)		Power discharge (W)	SEI (kJ L^{-1})	References
			CH$_4$	CO$_2$	H$_2$	CO			
DBD	50	1/1	30.0	19.2	8.7	10.0	50	*60.0*	[16]
DBD	200	4/1	64.0	54.0	52.0	14.0	1000	*300.0*	[12]
DBD	20	1/1	79.7	52.7	59.8	NR	NR	NR	[15]
Nanosecond pulsed discharge	100	3/2	30.0	NR	12.0	7.5	*10*	*6.3*	[2]
DC corona discharge (positive corona)	60	2/1	86.0	65.0	*55.7*	NR	45	*45.0*	[20]
Glow discharge	2200	6/4	61.0	49.9	*54.4*	NR	NR	NR	[17]
AC Gliding arc	7500	7/3	13.1	8.4	*4.1*	NR	NR	NR	[7]
Gliding arc Plasmatron	10,000	3/1	41.0	24.0	20.9	NR	500	3.0	[52]
Gliding arc	1000	1/1	40.0	31.0	*20.0*	NR	190	*11.4*	[24]
RGA	12,000	1/1	36.0	35.0	*9.8*	NR	471	*2.4*	[25]
RGA	6000	1/1	48.0	54.0	48.0	51.0	175	*1.8*	[30]
RGA	3700	1/1	10.9	12.8	8.7	7.5	155	6.7	This work

The italic fonts are calculated values, based on Eq. 16 for SEI (values divided by 22.4 L mol^{-1} to get kJ L^{-1})
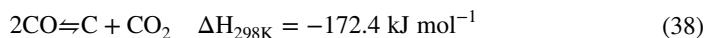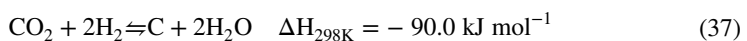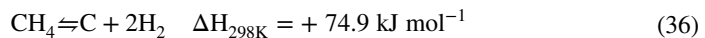
NR non-reported

Qualitative Analysis of the Optical Emission Spectrum

Figure 13 shows the characteristic optical emission spectra (200–700 nm) obtained for a RGA operating with $CO_2/CH_4 = 1.5$, total gas flow rate of 3.7 SLPM and peak currents of 0.74 and 1.50 A. Due to the strong molecular emissions from C_2 Swan bands (468–473, 500–516, and 530–563 nm), the arc appeared bright green. C_2 was formed during hydrocarbon degradation in the discharge [53] and is considered an indicator for nanostructured solid carbon formation [25]. We observed that increasing the relative concentration of CO_2 in the inlet gas mixture led to an overall decrease in the intensity of the C_2 Swan bands (spectra not reported here). The latest observation was confirmed visually as the visual appearance of the arc went from green to white when the amount of CO_2 in the inlet flow increased. Moreover, higher amount of H_2 was produced at lower CO_2 concentrations, i.e., $CO_2/CH_4 = 1.0$, meaning a reduced degree of dehydrogenated CH_4. CH bands were identified around 387 and 430 nm ($A^2\Delta \rightarrow X^2\prod$ transitions) [16], which according to Ray et al. [54] is due to the excitation of $C^2\sum^+ \rightarrow X^2\prod$ and indicates the formation of higher hydrocarbons (first band). Additionally, some molecular emission bands related to CO_2 were identified around 357, 374 and 435 nm [53, 55]. An intense emission line was observed at 588.7 nm, which is most likely attributed to carbon ions, C^+ [56]. The H_α emission line was also observed at 656 nm, whereas a weak emission band for CO was identified at 283 nm [16, 53]. These reactive species participate directly in the reforming reaction where CO_2 and CH_4 are ionized and dissociated to produce ions and radicals that interact and convert mainly into CO and H_2.

Morphology of the Deposited Particulates

One of the main drawbacks of DRM is the occurrence of carbon deposition. This process is unavoidable and thermodynamically favored [39] as shown by Eqs. (36–38)

$$CH_4 \leftrightharpoons C + 2H_2 \quad \Delta H_{298K} = +74.9 \text{ kJ mol}^{-1} \tag{36}$$

$$CO_2 + 2H_2 \leftrightharpoons C + 2H_2O \quad \Delta H_{298K} = -90.0 \text{ kJ mol}^{-1} \tag{37}$$

$$2CO \leftrightharpoons C + CO_2 \quad \Delta H_{298K} = -172.4 \text{ kJ mol}^{-1} \tag{38}$$

Equation (36) is known as methane cracking or methane pyrolysis; Eq. (37) involves steam generation via CO_2 reforming, i.e., CO_2 reduction, whereas Eq. (38) is the Boudouard

Fig. 13 Emission spectra observed in the RGA for DRM at $CO_2/CH_4 = 1.5$, a total flow rate of 3.7 SLPM and peak currents of 0.74 (less intense) and 1.50 A (more intense)
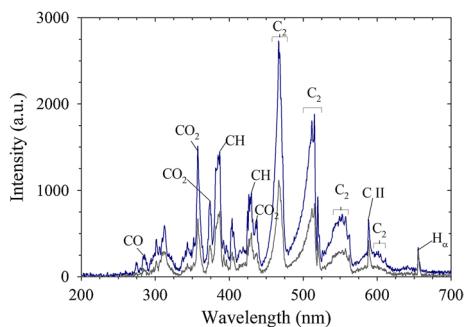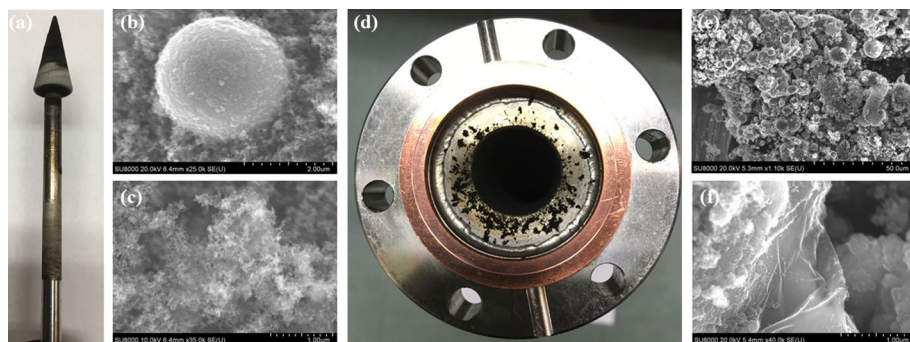
Fig. 14 Left: **a** stainless steel cathode covered with black carbon, a by-product of DRM, **b** stainless steel particle found in the black carbon, as a result of electrode erosion, **c** black carbon. On the right: **d** top view of the stainless steel anode with some black carbon powder, **e** black carbon and stainless steel particles, **f** carbon structure
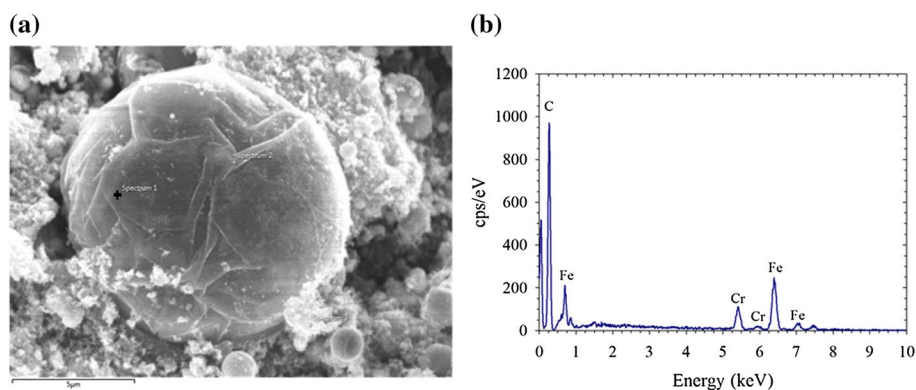

Fig. 15 **a** Stainless steel particle from the anode covered by a carbon-containing structure, **b** EDS spectrum of the stainless steel particle. The cross in **a** shows the exact location where the EDS analysis was carried out

reaction (opposite of Eq. 5) [6, 29]. According to their origin, two different types of deposits can be identified: solid carbon and coke. Solid carbon is a product of CO-disproportionation, whilst coke occurs as decomposition or condensation of hydrocarbons on the catalyst surface [57]. Carbon deposition depends on the CO_2/CH_4 ratio, being favored at lower ratio [7]. The methane decomposition process not only leads to higher production of H_2 but also to more solid carbon deposited on the electrodes [39]. Particulate deposition was observed not only on both electrodes (Fig. 14) but also in the upper and colder sections of the reactor, towards the gas exhaust. Furthermore, micron-sized particles of stainless steel, mostly produced by arc erosion of the cathode, were found in the deposits (confirmed with Energy Dispersive X-ray Spectroscopy (EDS)). In the samples collected on the anode surface (Figs. 14e, 15), the stainless-steel microparticles were mostly covered by a carbon-containing structure (Figs. 14f, 15).

Carbon samples collected from the cathode were also analyzed by Raman spectroscopy (Fig. 16). The D, G, and G'-bands can be clearly identified. The D-band at 1327 cm^{-1} corresponds to the amorphous carbon (non-graphitized) and disordered structure. The G-band

Fig. 16 Raman spectrum of one carbon sample produced during the DRM reaction by the RGA discharge after approx. 20 h
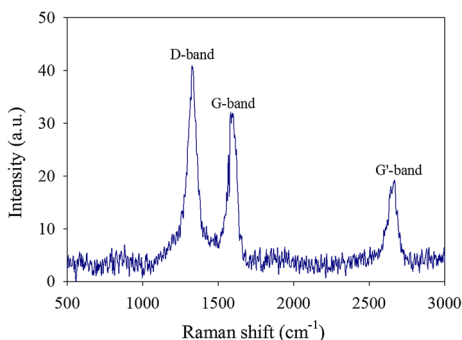
at 1582 cm^{-1} is linked to the tangential mode of the graphene sheet and graphitized structure [7, 25]. Finally, the G'-band, also known as the 2D band, at 2665 cm^{-1} is the result of different interlayer interactions occurring at different depths within the graphene [58]. The intensity of the D band relative to the G band quantifies the degree of crystallinity of the graphite layers, in this study $I_D/I_G = 1.5$, which suggests a low degree of graphitization [7].

Conclusions

An atmospheric pressure rotating gliding arc co-driven by a magnetic field has been developed for the plasma-assisted dry reforming of the methane reaction. Operating parameters such as total gas flow rate, peak arc current, and CO_2/CH_4 ratio were varied to determine the most efficient combination for dry reforming of methane. The RGA discharge has shown to be a good plasma source in the generation of cleaner syngas, as only trace concentrations of by-products were found in the effluent gas, whereas the carbon balance was > 95% for all the combinations of parameters studied. The optical emission spectrum showed the formation of active species in the plasma zone that are involved in the DRM, such as H_α, C_2, CH, C^+, and CO_2. The results suggested that plasma acts as a catalyst in the generation of H_2 and CO, where the yield of these products presented a transient behavior in the first minutes to finally stabilized. These results can possibly be used to determine the best time to measure the gas concentrations, especially when sampling offline. Moreover, increasing the peak current mostly increased the conversions of CH_4 and CO_2 and the by-products concentration, such as C_2H_2 and solid carbon. However, increasing the flow rate led to a decrease in CO_2 and CH_4 conversions. Conversely, when the arc current was set at 0.74 A, an increase of the flow rate from 3.7 to 4.7 SLPM seemed to be beneficial for CO_2 and CH_4 conversions for $CO_2/CH_4 = 1.0$ and 1.5 as the increase in the arc length enhanced the conversion. Besides, vibrational excitation could lead to CO_2 activation in a more efficient pathway. This explanation also applied for a peak current of 1.50 A and $CO_2/CH_4 = 2.0$. On the other hand, the H_2/CO_2 ratio was inversely proportional to the CO_2/CH_4 ratio, i.e., the higher the CO_2 concentration in the reactive gas, the lower the H_2 produced. No significant effect of the peak current or flow rate was found in the H_2/CO ratio. Increasing the energy input by preheating the gas inlet did not show a significant effect on the CH_4 and CO_2 conversions as well as the H_2 and CO yields, as the gas temperatures in the plasma zone are much higher (1000–3000 K) compared to the preheated gas temperature (200 °C, 473 K). On the other hand, the plasma discharge induced gas heating,

resulting in an increased temperature of roughly 200 K. For the larger peak current, i.e., 1.50 A, the best energy efficiency values were obtained at the lowest specific energy input values. Higher values of energy efficiency were obtained at lower flow rates and higher CO_2/CH_4 ratios. As a result of electrode erosion, microparticles of stainless-steel with a structure containing carbon were obtained as a by-product of DRM in the RGA. Raman spectroscopy suggested that the carbon deposits contain amorphous carbon and graphene sheets, which can be potentially useful in industrial/research applications, adding value to the DRM process. Further studies are needed to identify better the nature of the carbon structures. Further work focuses on the addition of a fluidized bed of catalyst for the plasma-catalytic DRM reaction.

Compliance with Ethical Standards

Conflict of interest The authors declare that they have no conflict of interest.

References

1. Pakhare D, Spivey J, Zhao H et al (2014) A review of dry (CO_2) reforming of methane over noble metal catalysts. Chem Soc Rev 43:7813–7837. https://doi.org/10.1039/C3CS60395D
2. Maqueo PDG, Coulombe S, Bergthorson JM (2019) Energy efficiency of a nanosecond repetitively pulsed discharge for methane reforming. J Phys D Appl Phys. https://doi.org/10.1088/1361-6463/ab199b
3. North American Power Plant Air Emissions (2011). Montreal, Quebec, Canada
4. NASA: Global Climate Change (2018) Climate change: how do we know? https://climate.nasa.gov/evidence/. Accessed 28 Jun 2018
5. National Academy of Sciences (2014) Climate change: evidence and causes. National Academies Press, Washington
6. Lavoie J-M (2014) Review on dry reforming of methane, a potentially more environmentally-friendly approach to the increasing natural gas exploitation. Front Chem 2:81. https://doi.org/10.3389/fchem.2014.00081
7. Tu X, Whitehead JC (2014) Plasma dry reforming of methane in an atmospheric pressure AC gliding arc discharge: co-generation of syngas and carbon nanomaterials. Int J Hydrog Energy 39:9658–9669. https://doi.org/10.1016/j.ijhydene.2014.04.073
8. Tan Z, Ai P (2017) CO_2 reforming of biogas to obtain synthesis gas using non-thermal plasma. J Energy Inst 90:864–874. https://doi.org/10.1016/J.JOEI.2016.08.008
9. Olsbye U, Wurzel T, Mleczko L (1997) Kinetic and reaction engineering studies of dry reforming of methane over a Ni/La/Al_2O_3 catalyst. Ind Eng Chem Res 35:5180–5188. https://doi.org/10.1021/ie9702461
10. Liu J-L, Park H-W, Chung W-J, Park D-W (2016) High-efficient conversion of CO_2 in AC-pulsed tornado gliding arc plasma. Plasma Chem Plasma Process 36:437–449. https://doi.org/10.1007/s11090-015-9649-2
11. Chen G, Georgieva V, Godfroid T et al (2016) Plasma assisted catalytic decomposition of CO_2. Appl Catal B Environ 190:115–124. https://doi.org/10.1016/j.apcatb.2016.03.009
12. Zhou LM, Xue B, Kogelschatz U, Eliasson B (1998) Nonequilibrium plasma reforming of greenhouse gases to synthesis gas. Energy Fuels 12:1191–1199. https://doi.org/10.1021/ef980044h

13. Brock SL, Shimojo T, Suib SL et al (2002) Application of non-thermal atmospheric pressure ac plasmas to the carbon dioxide reforming of methane. Res Chem Intermed 28:13–24. https://doi.org/10.1163/156856702760129465

14. Tu X, Gallon HJ, Whitehead JC (2013) Plasma-assisted reduction of a NiO/Al$_2$O$_3$ catalyst in atmospheric pressure H$_2$/Ar dielectric barrier discharge. Catal Today 211:120–125. https://doi.org/10.1016/j.cattod.2013.03.024

15. Wang Q, Yan B-H, Jin Y, Cheng Y (2009) Investigation of dry reforming of methane in a dielectric barrier discharge reactor. Plasma Chem Plasma Process 29:217–228. https://doi.org/10.1007/s11090-009-9173-3

16. Tu X, Whitehead JC (2012) Plasma-catalytic dry reforming of methane in an atmospheric dielectric barrier discharge: understanding the synergistic effect at low temperature. Appl Catal B Environ 125:439–448. https://doi.org/10.1016/j.apcatb.2012.06.006

17. Li D, Li X, Bai M et al (2009) CO$_2$ reforming of CH$_4$ by atmospheric pressure glow discharge plasma: a high conversion ability. Int J Hydrog Energy 34:308–313. https://doi.org/10.1016/j.ijhydene.2008.10.053

18. Cheng D-G, Zhu X, Ben Y et al (2006) Carbon dioxide reforming of methane over Ni/Al$_2$O$_3$ treated with glow discharge plasma. Catal Today 115:205–210. https://doi.org/10.1016/j.cattod.2006.02.063

19. Aziznia A, Bozorgzadeh HR, Seyed-Matin N et al (2012) Comparison of dry reforming of methane in low temperature hybrid plasma-catalytic corona with thermal catalytic reactor over Ni/γ-Al$_2$O$_3$. J Nat Gas Chem 21:466–475. https://doi.org/10.1016/S1003-9953(11)60392-7

20. Li M-W, Xu G-H, Tian Y-L et al (2004) Carbon dioxide reforming of methane using DC corona discharge plasma reaction. J Phys Chem A 108:1687–1693. https://doi.org/10.1021/jp037008q

21. Chen Q, Yang X, Sun J et al (2017) Pyrolysis and oxidation of methane in a RF plasma reactor. Plasma Chem Plasma Process 37:1551–1571. https://doi.org/10.1007/s11090-017-9844-4

22. Pacheco J, Soria G, Valdivia R et al (2014) Warm plasma reactor with vortex effect enhanced used for CH$_4$–CO$_2$ reforming. IEEE Trans Plasma Sci 42:2800–2801. https://doi.org/10.1109/TPS.2014.2337290

23. Sreethawong T, Thakonpatthanakun P, Chavadej S (2007) Partial oxidation of methane with air for synthesis gas production in a multistage gliding arc discharge system. Int J Hydrog Energy 32:1067–1079. https://doi.org/10.1016/j.ijhydene.2006.07.013

24. Indarto A, Choi J-W, Lee H, Song HK (2006) Effect of additive gases on methane conversion using gliding arc discharge. Energy 31:2986–2995. https://doi.org/10.1016/j.energy.2005.10.034

25. Wu A, Yan J, Zhang H et al (2014) Study of the dry methane reforming process using a rotating gliding arc reactor. Int J Hydrog Energy 39:17656–17670. https://doi.org/10.1016/J.IJHYDENE.2014.08.036

26. Li K, Liu J-L, Li X-S et al (2016) Warm plasma catalytic reforming of biogas in a heat-insulated reactor: dramatic energy efficiency and catalyst auto-reduction. Chem Eng J 288:671–679. https://doi.org/10.1016/j.cej.2015.12.036

27. Zhang H, Du C, Wu A et al (2014) Rotating gliding arc assisted methane decomposition in nitrogen for hydrogen production. Int J Hydrog Energy 39:12620–12635. https://doi.org/10.1016/J.IJHYDENE.2014.06.047

28. Chen HL, Lee HM, Chen SH et al (2008) Review of plasma catalysis on hydrocarbon reforming for hydrogen production—interaction, integration, and prospects. Appl Catal B Environ 85:1–9. https://doi.org/10.1016/j.apcatb.2008.06.021

29. Chung W-C, Chang M-B (2016) Review of catalysis and plasma performance on dry reforming of CH4 and possible synergistic effects. Renew Sustain Energy Rev 62:13–31. https://doi.org/10.1016/j.rser.2016.04.007

30. Pacheco J, Soria G, Pacheco M et al (2015) Greenhouse gas treatment and H2 production, by warm plasma reforming. Int J Hydrog Energy 40:17165–17171. https://doi.org/10.1016/j.ijhydene.2015.08.062

31. Neyts EC (2016) Plasma-surface interactions in plasma catalysis. Plasma Chem Plasma Process 36:185–212. https://doi.org/10.1007/s11090-015-9662-5

32. Zhang H, Li L, Li X et al (2018) Warm plasma activation of CO$_2$ in a rotating gliding arc discharge reactor. J CO2 Util 27:472–479. https://doi.org/10.1016/J.JCOU.2018.08.020

33. Fridman A, Gutsol A, Gangoli S et al (2008) Characteristics of gliding arc and its application in combustion enhancement. J Propuls Power 24:1216–1227. https://doi.org/10.2514/1.24795

34. Fridman A, Nester S, Kennedy LA (1999) Gliding arc gas discharge. Prog Energy Combust Sci 25:211–231. https://doi.org/10.1016/S0360-1285(98)00021-5

35. Zhang H, Li XD, Zhang YQ et al (2012) Rotating gliding arc codriven by magnetic field and tangential flow. IEEE Trans Plasma Sci 40:3493–3498. https://doi.org/10.1109/TPS.2012.2220984

36. Hwang N, Lee J, Lee DH, Song Y-H (2012) Interactive phenomena of a rotating arc and a premixed CH$_4$ flame. Plasma Chem Plasma Process 32:187–200. https://doi.org/10.1007/s11090-012-9349-0
37. McNall M, Coulombe S (2018) Characterization of a rotating gliding arc in argon at atmospheric pressure. J Phys D Appl Phys. https://doi.org/10.1088/1361-6463/aade44
38. Lesueur H, Czernichowski A, Chapelle J (1994) Electrically assisted partial oxidation of methane. Int J Hydrog Energy 19:139–144. https://doi.org/10.1016/0360-3199(94)90118-X
39. Nikoo MK, Amin NAS (2011) Thermodynamic analysis of carbon dioxide reforming of methane in view of solid carbon formation. Fuel Process Technol 92:678–691. https://doi.org/10.1016/j.fuproc.2010.11.027
40. Bo Z, Yan J, Li X et al (2008) Plasma assisted dry methane reforming using gliding arc gas discharge: effect of feed gases proportion. Int J Hydrog Energy 33:5545–5553. https://doi.org/10.1016/j.ijhydene.2008.05.101
41. Lu N, Sun D, Xia Y et al (2018) Dry reforming of CH4-CO2 in AC rotating gliding arc discharge: effect of electrode structure and gas parameters. Int J Hydrog Energy 43:13098–13109. https://doi.org/10.1016/J.IJHYDENE.2018.05.053
42. Istadi ANAS (2006) Co-generation of synthesis gas and C$_{2+}$ hydrocarbons from methane and carbon dioxide in a hybrid catalytic-plasma reactor: a review. Fuel 85:577–592. https://doi.org/10.1016/j.fuel.2005.09.002
43. Bogaerts A, Berthelot A, Heijkers S et al (2017) CO$_2$ conversion by plasma technology: insights from modeling the plasma chemistry and plasma reactor design. Plasma Sources Sci Technol 26:063001
44. Czernichowski A (2001) Glidarc assisted preparation of the synthesis gas from natural and waste hydrocarbons gases. Oil Gas Sci Technol 56:181–198. https://doi.org/10.2516/ogst:2001018
45. Liu C-J, Xu G-H, Wang T (1999) Non-thermal plasma approaches in CO utilization. Fuel Process Technol 58:119–134
46. Sun SR, Wang HX, Mei DH et al (2017) CO2 conversion in a gliding arc plasma: Performance improvement based on chemical reaction modeling. J CO2 Util 17:220–234. https://doi.org/10.1016/j.jcou.2016.12.009
47. Sudhakaran MSP, Trinh HQ, Karuppiah J et al (2017) Plasma catalytic removal of p-xylene from air stream using γ-Al$_2$O$_3$ supported manganese catalyst. Top Catal 60:944–954. https://doi.org/10.1007/s11244-017-0759-3
48. Hammer T, Kappes T, Baldauf M (2004) Plasma catalytic hybrid processes: gas discharge initiation and plasma activation of catalytic processes. Catal Today 89:5–14. https://doi.org/10.1016/j.cattod.2003.11.001
49. Eliasson B, Liu C-J, Kogelschatz U et al (2000) Direct conversion of methane and carbon dioxide to higher hydrocarbons using catalytic dielectric-barrier discharges with zeolites. Ind Eng Chem Res. https://doi.org/10.1021/ie990804r
50. Ghorbanzadeh AM, Lotfalipour R, Rezaei S (2009) Carbon dioxide reforming of methane at near room temperature in low energy pulsed plasma. Int J Hydrog Energy 34:293–298. https://doi.org/10.1016/j.ijhydene.2008.10.056
51. Scapinello M, Martini LM, Dilecce G, Tosi P (2016) Conversion of CH$_4$/CO$_2$ by a nanosecond repetitively pulsed discharge. J Phys D Appl Phys. https://doi.org/10.1088/0022-3727/49/7/075602
52. Cleiren E, Heijkers S, Ramakers M, Bogaerts A (2017) Dry reforming of methane in a gliding arc plasmatron: towards a better understanding of the plasma chemistry. Chemsuschem 10:4025–4036. https://doi.org/10.1002/cssc.201701274
53. Kraus M, Egli W, Haffner K et al (2002) Investigation of mechanistic aspects of the catalytic CO$_2$ reforming of methane in a dielectric-barrier discharge using optical emission spectroscopy and kinetic modeling. Phys Chem Chem Phys 4:668–675. https://doi.org/10.1039/b108040g
54. Ray D, Manoj P, Reddy K et al (2017) Ni-Mn/γ-Al2O3 assisted plasma dry reforming of methane. Catal Today 309:212–218. https://doi.org/10.1016/j.cattod.2017.07.003
55. Ray D, Subrahmanyam C (2016) CO$_2$ decomposition in a packed DBD plasma reactor: influence of packing materials. RSC Adv 6:39492–39499. https://doi.org/10.1039/C5RA27085E
56. Fazekas P, Keszler AM, Bódis E et al (2015) Optical emission spectra analysis of thermal plasma treatment of poly(vinyl chloride). Open Chem 13:549–556. https://doi.org/10.1515/chem-2015-0069
57. Kopyscinski J (2010) Production of synthetic natural gas in a fluidized bed reactor. ETH Zurich, Zürich
58. Hodkiewicz J (2010) Characterizing carbon materials with Raman spectroscopy. Madison,WI, USA